Available online at www.sciencedirect.com
SCIENCE DIRECT®
International Journal of Heat and Mass Transfer 47 (2004) 3841–3854
International Journal of HEAT and MASS TRANSFER
www.elsevier.com/locate/ijhmt

Direct-contact evaporation in the homogeneous and heterogeneous bubbling regimes. Part II: dynamic simulation

Cláudio P. Ribeiro Jr., Paulo L.C. Lage *

Programa de Engenharia Química—COPPE, Universidade Federal do Rio de Janeiro, P.O. Box 68502, 21945-970 Rio de Janeiro, RJ, Brazil

Received 5 June 2003; received in revised form 15 March 2004
Available online 6 May 2004

Abstract

Considering the bimodal feature of the bubble size distribution in the heterogeneous regime, a recently developed model for simulating direct-contact evaporators operating in the homogeneous regime was extended to the heterogeneous bubbling regime, enabling, thereby, the simulation of a direct-contact evaporator for any bubbling regime. The proposed model includes a correction factor for isothermal gas hold-up correlations to account for heat and mass transfer effects which arise in non-isothermal bubbling. The model predictions were shown to be in good agreement with literature experimental data for the air–water system, considering four different gas superficial velocities.

Keywords: Heat and mass transfer; Direct-contact evaporator; Gas hold-up; Bubble column; Simulation

1. Introduction

In a direct-contact evaporator, liquid vaporisation is brought about by the dispersion of a superheated gas in the solution to be concentrated. The lack of any walls separating the processing streams imparts many advantages to direct-contact units in comparison with the traditional shell-and-tube evaporators, such as higher thermal efficiency, lower capital and operating costs and greater simplicity of construction. In particular, the possibility to operate economically with highly fouling and/or corrosive solutions has led to the successful application of this kind of evaporator to a wide variety of processing problems [1,2].

In a companion paper [3], an experimental investigation of the heat and mass transfer processes in a bench scale direct-contact evaporator was conducted. Contrary to what was done in previously published works [4–6], operation was not restricted to the homogeneous bubbling regime, as some of the analysed gas superficial velocities were high enough to enable operation in the heterogeneous bubbling regime. Significant effects of both the sparger and the gas flow rate upon the equipment performance were verified and systematically analysed.

Attention is now focused on the mathematical modelling of direct-contact evaporators. In these units, for semi-batch operation, the time interval required for the quasi-steady-state regime to be achieved, at which the liquid temperature and the evaporation rate remain approximately constant, usually has the magnitude of hours. On the other hand, the bubble residence time in the equipment equals some seconds. Therefore, a time scale decomposition can be performed in the modelling of direct-contact evaporators [7], resulting in a distinct dynamic model for each phase.

The consideration of a single bubble size in the dispersed phase seems to be a common feature of all models which have been proposed so far for the simulation of direct-contact evaporators [4–6,8–10]. Even when the variation of the bubble size due to the density increase, which comes from the steep decrease in the gas temperature, is taken into account using either

* Corresponding author. Tel.: +55-21-2562-8346; fax: +55-21-2562-8300.
E-mail address: paulo@peq.coppe.ufrj.br (P.L.C. Lage).

0017-9310/$ - see front matter © 2004 Elsevier Ltd. All rights reserved.
doi:10.1016/j.ijheatmasstransfer.2004.03.017

Nomenclature

C_D	drag coefficient
Cp	specific heat at constant pressure ($J\,kg^{-1}\,K^{-1}$)
D	mass diffusion coefficient ($m^2\,s^{-1}$)
D_c	evaporator inner diameter (m)
D_e	evaporator outer diameter (m)
D_{isl}	external diameter of the insulated evaporator (m)
d_e	equivalent diameter of the sphere with the same volume of the bubble (m)
d_h	hydraulic bubble diameter (m)
Eo	Eötvös number ($gd_e^2(\rho_L - \rho_G)\sigma^{-1}$)
f_1	correction factor for population effect
f_2	correction factor for wall effect
f_2^*	parameter defined by Eq. (13a)
F_D	drag force (N)
f_o	frequency of bubble formation at an orifice (s^{-1})
g	gravity acceleration ($m\,s^{-2}$)
G	volumetric flow rate ($m^3\,s^{-1}$)
h	heat-transfer coefficient ($W\,m^{-2}\,K^{-1}$)
H_b	two-phase mixture overall height in the evaporator (m)
H_c	column height (m)
ΔH_{vap}	latent heat of vaporisation ($J\,kg^{-1}$)
m_b	bubble mass (kg)
$\dot{m}_{ev}$	bubble evaporation rate ($kg\,s^{-1}$)
m_{ev}	mass of vaporised liquid per bubble (kg)
m_L	liquid mass in the evaporator (kg)
M	mass flow rate ($kg\,s^{-1}$)
n_{sb}	number of 'small' bubbles needed to originate one 'large' bubble
N_o	number of orifices in the sparger
q_s	total amount of sensible heat transferred to the liquid per bubble (J)
Q	heat-transfer rate (W)
r	radial coordinate (m)
R	bubble radius (m)
Re	Reynolds number, ($u_b d_e v^{-1}$)
R_{exp}	large bubble radius at the beginning of the ascension stage (m)
t	time (s)
T	temperature (K)
u_b	bubble velocity ($m\,s^{-1}$)
u_G	gas superficial velocity ($m\,s^{-1}$)
u_{trans}	gas superficial velocity at bubbling regime transition ($m\,s^{-1}$)
U	overall heat-transfer coefficient ($W\,m^{-2}\,K^{-1}$)
v	radial velocity ($m\,s^{-1}$)
V	volume (m^3)
X	mass fraction in the liquid phase
Y	mass fraction in the gas phase

Greek symbols

δ	unit impulse function (Dirac delta function) (m^{-3})
ε	gas hold-up
ϑ	ratio between the bubble and the column diameters
λ	thermal conductivity ($W\,m^{-1}\,K^{-1}$)
ν	kinematic viscosity ($m\,s^{-2}$)
ρ	density ($kg\,m^{-3}$)
σ	surface tension ($N\,m^{-1}$)
ψ	ratio between the real and hypothetical gas volumes

Subscripts

∞	isolated bubble in an infinite medium
amb	evaporator surroundings
asc	ascension stage
c	evaporator wall
cond	condensate stream in the upper region of the evaporator
d	sparger
ev	evaporated from the liquid phase
ext	outside the bubble
feed	evaporator feed stream
form	formation stage
G	gas
hyp	hypothetical isothermal bubbling process
I	injected gas
i	species i (1 for water vapour)
isl	evaporator insulating material
L	liquid
lb	large bubble
out	evaporator outlet stream
p	losses to the surroundings
res	residence in the evaporator
s	superheated gas
sb	small bubble
sur	surface

Superscripts

—	mean property
~	partial mass property
0	pure component
fb	freeboard region of the evaporator
lb	large bubble
sb	small bubble

experimental bubble sizes [6] or incorporating such effect in the model for bubble formation and ascension [10], the identity of the bubble is kept constant throughout the process. These hypotheses represent well the pattern observed in the homogeneous bubbling regime, in which there is no great difference between the size of the bubbles and the breakage and coalescence phenomena are negligible. Industrially, however, the homogenous regime is less likely to prevail, owing to the high gas flow rates employed, which favour the heterogeneous bubbling regime, whose intrinsic characteristics, that is, wide range of bubble sizes and non-negligible frequencies of breakage and coalescence, invalidate the consideration of a single bubble size.

In this paper, a mathematical model for the dynamic simulation of direct-contact evaporators operating in the heterogeneous bubbling regime is presented. Its main feature is the representation of the heterogeneous regime using a simplified fluid dynamic approach, originally proposed by Vermeer and Krishna [11] for bubble columns, which is based upon the division of the bubble population into two classes. The adoption of this simplified approach was encouraged by the favourable results exhibited by some semi-empirical gas hold-up models which employ this concept [12–15].

2. Model development

The proposed model actually constitutes an extension to the heterogeneous regime of the model developed by Campos and Lage [10] for direct-contact evaporators operating in the homogeneous bubbling regime. Its basic assumption is the division of the dispersed phase into two bubble sizes which do not interact: the 'small' bubbles, generated by the sparger, and the 'large' bubbles, produced by the coalescence of the former. For each bubble size, the heat and mass transfer rates are determined for the respective residence time within the equipment, which are, then, weighted to give the results associated with the dispersed phase.

The differences between the bubbling processes related to each kind of bubble are portrayed in Fig. 1a. Assuming that the sparger orifices are sufficiently

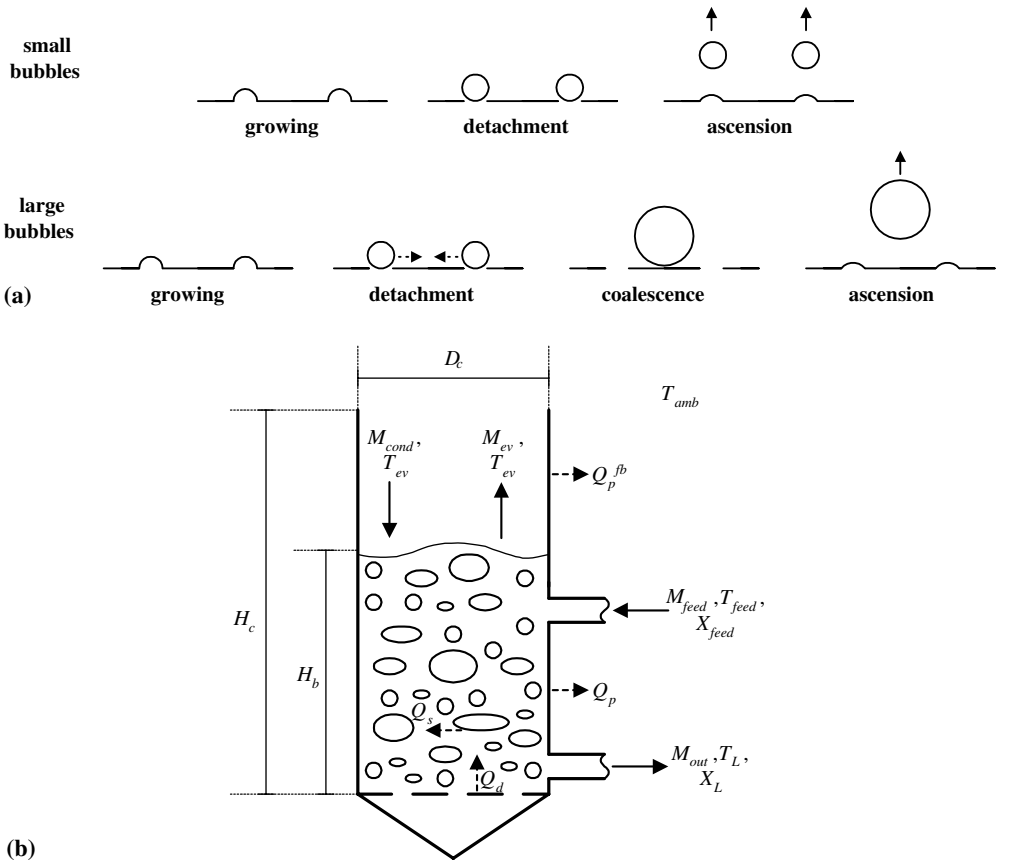

Fig. 1. Direct-contact evaporator model: (a) stages of the bubbling process for the two kinds of bubbles considered; (b) schematic representation of the analysed unit, indicating the mass (continuous lines) and heat (dashed lines) transfer rates.

spaced, coalescence is restricted to the ascension stage, so that the formation stage (growing + detachment) is the same for both kinds of bubbles. Once the formation volume has been achieved, the 'small' bubble detaches and the ascension stage commences. As regards the 'large' bubble, the volume at the end of the formation stage is the same but, after the detachment, the occurrence of an instantaneous coalescence process is postulated for the formation of the 'large' bubble, which, then, ascends in the column. The size of the 'large' bubble has to be experimentally determined and constitutes an input parameter of the present model.

2.1. Dispersed phase model

Experimental evidences [9,16–18] indicate that the major resistance to heat and mass transfer lies within the bubbles and, hence, the dispersed phase modelling has drawn considerable attention. As a result, many models for describing coupled heat and mass transfer in bubbles have already been elaborated, either for the formation [19–24] or the ascension stage [4–6,8,9,25–27]. However, to the authors' knowledge, the only available model valid for both the formation and ascension stages is the one proposed by Campos and Lage [28], which was, hence, chosen for representing the heat and mass transfer phenomena in the bubbles.

In the formation stage, there is no difference whatsoever between the two kinds of bubbles and, as a result, the model of Campos and Lage [28] is directly applied. It is constituted of the following simplified forms of the continuity, species and energy conservation equations for the bubble, which is assumed to be a binary mixture:

$$\frac{\partial \rho_G}{\partial t} + \frac{1}{r^2}\frac{\partial}{\partial r}(r^2 \rho_G v) = \rho_I G_I \delta(r) \tag{1}$$

$$\frac{\partial}{\partial t}(\rho_G Y_i) + \frac{1}{r^2}\frac{\partial}{\partial r}\left[r^2 \rho_G \left(Y_i v - D_i \frac{\partial Y_i}{\partial r}\right)\right] = \rho_I G_I Y_{i_I} \delta(r) \tag{2}$$

$$\frac{\partial}{\partial t}(\rho_G Cp_G T) + \frac{1}{r^2}\frac{\partial}{\partial r}(r^2 \rho_G v Cp_G T) - \frac{1}{r^2}\frac{\partial}{\partial r}\left(r^2 \lambda_G \frac{\partial T}{\partial r}\right) - (\overline{Cp_1^0} - \overline{Cp_2^0})\frac{1}{r^2}\frac{\partial}{\partial r}\left(r^2 T \rho_G D_1 \frac{\partial Y_1}{\partial r}\right) = \rho_I G_I \delta(r) \sum_{i=1}^{2} Y_{i_I} \overline{Cp_i^0} T_I \tag{3}$$

being the index 1 related to water. Eqs. (1)–(3) are subjected to the following boundary conditions:

$$\frac{-\dot{m}_{ev}}{4\pi R^2} = \rho_G \left(v - \frac{dR}{dt}\right) \quad \text{at } r = R(t) \tag{4a}$$

$$\rho_G D_1 \left.\frac{\partial Y_1}{\partial r}\right|_{r=R(t)} = \frac{\dot{m}_{ev}}{4\pi R^2}(1 - Y_1) \quad \text{at } r = R(t) \tag{4b}$$

$$-\lambda_G \left.\frac{\partial T}{\partial r}\right|_{r=R(t)} = \frac{\dot{m}_{ev}}{4\pi R^2}\Delta H_{vap}(T) + h_{ext}(T - T_L) \quad \text{at } r = R(t) \tag{4c}$$

as well as the following initial conditions

$$\rho_G(r,0) = \rho_I, \quad Y_1(r,0) = Y_{1_I}, \quad T(r,0) = T_I \quad \forall r \tag{5}$$

being h_{ext} calculated using the correlation of Calderbank and Moo-Young [29].

In order to predict the moment of detachment, Eqs. (1)–(3) have to be solved together with a dynamic model for bubble formation. In this work, as done by Campos and Lage [28], the dynamic model of Davidson and Schüler [30] was used in view of the recommendations of Pinto [22]:

$$\frac{du_b}{dt} + 3\frac{u_b}{R}\frac{dR}{dt} = \frac{16}{11}g - \frac{72}{11}\frac{\nu_L u_b}{R^2} \tag{6}$$

In the ascension stage, the conservation equations are obtained by eliminating the injection terms from Eqs. (1)–(3), that is, by setting the right-hand side of these equations to zero. The boundary conditions at the bubble surface are the same as the ones for the formation stage, Eqs. (4a)–(4c).

The differences between the two kinds of bubbles lie in the initial conditions for solving the conservation equations. For the 'small' bubble, as ascension takes place immediately after formation, the profiles associated with the end of the latter naturally constitute the initial conditions of the former, that is:

$$R(0)|_{asc,sb} = R(t_{form}) \tag{7a}$$

$$\begin{aligned} \rho_G(r,0)|_{asc,sb} &= \rho_G(r, t_{form}) \\ Y_1(r,0)|_{asc,sb} &= Y_1(r, t_{form}) \\ T(r,0)|_{asc,sb} &= T(r, t_{form}) \quad \forall r \end{aligned} \tag{7b}$$

However, with regard to the 'large' bubble, the coalescence process which occurs after the detachment produces two modifications. First and more evidently, the bubble radius changes. Moreover, as a result of the intense internal mixing which should accompany a coalescence process, there is a perturbation in the profiles established in the formation stage. As a limit case, this mixing is assumed to be high enough to eliminate all internal temperature and concentration gradients. Consequently, at the beginning of the ascension stage, both the temperature and the vapour concentration inside the bubble do not depend upon the radial position, being equal to the corresponding mean of the values at the end of the formation stage:

$$R(0)|_{asc,lb} = R_{exp} \tag{8a}$$

$$Y_1(r,0)|_{\text{asc,lb}} = \int_0^{R(t_{\text{form}})} \rho_{\text{G}}(\zeta,t_{\text{form}})Y_1(\zeta,t_{\text{form}})\zeta^2\,\mathrm{d}\zeta \times \left[\int_0^{R(t_{\text{form}})} \rho_{\text{G}}(\zeta,t_{\text{form}})\zeta^2\,\mathrm{d}\zeta\right]^{-1} \quad \forall r \quad (8b)$$

$$T(r,0)|_{\text{asc,lb}} = \int_0^{R(t_{\text{form}})} \rho_{\text{G}}(\zeta,t_{\text{form}})Cp(\zeta,t_{\text{form}})T(\zeta,t_{\text{form}})\zeta^2\,\mathrm{d}\zeta \times \left[\int_0^{R(t_{\text{form}})} \rho_{\text{G}}(\zeta,t_{\text{form}})Cp(\zeta,t_{\text{form}})\zeta^2\,\mathrm{d}\zeta\right]^{-1} \quad \forall r \quad (8c)$$

Once the new values of Y_1 and T are known, the bubble density is computed using the ideal gas model. It ought to be emphasised that the radius of the 'large' bubble at the beginning of the ascension stage, R_{exp}, is an input parameter of the model.

Whichever the kind of the bubble, its dynamics in the ascension stage is described by a force balance taking into account inertial, added mass, buoyancy and drag forces:

$$\frac{\mathrm{d}}{\mathrm{d}t}\left[\left(m_{\text{b}} + \frac{4}{6}\pi R^3\rho_{\text{L}}\right)u_{\text{b}}\right] = \frac{4}{3}\pi R^3 g(\rho_{\text{L}} - \rho_{\text{G}}) - F_{\text{D}} \quad (9)$$

In Eq. (9), u_{b} represents the 'real' bubble velocity, corrected for population and wall effects, both of which were not considered by Campos and Lage [28] in their original model. Therefore, in the calculation of the drag force, F_{D}, an expression including these two effects has to be employed. In the literature, however, the common approach to account for such effects is to apply a correction factor for the velocity of the isolated bubble, $u_{\text{b}\infty}$, so that these factors had to be manipulated in order to obtain an expression for the corresponding drag force.

When the bubble reaches its terminal ascension velocity, the buoyancy and drag forces become equal. Since buoyancy does not depend on wall and population effects, one concludes that, once the terminal velocity has been achieved, the drag force will be the same for either the isolated or 'real' (subjected to population and wall effects) bubble. Expressing the drag force using the formula of Karamanev [31], which explicitly includes the shape of the bubble by means of the ratio between the equivalent diameter (d_{e}) and the hydraulic diameter of the bubble (d_{h}), one has:

$$F_{\text{D}} = 0.5\pi R^2\rho_{\text{L}}u_{\text{b}}^2C_{\text{D}}(Re)(d_{\text{h}}/d_{\text{e}})^2 \quad (10)$$

Considering that $u_{\text{b}} = u_{\text{b}\infty}f_1(\varepsilon)f_2(\vartheta)$, where $f_1(\varepsilon)$ and $f_2(\vartheta)$ are, respectively, the correction factors for population and wall effects, it can be seen that, if the drag force is the same and the differences in the bubble shape factors are neglected, the reduction in the value of u_{b} has to be compensated by an increase in the C_{D} value, so that the product $u_{\text{b}}^2C_{\text{D}}$ remains the same. Hence:

$$C_{\text{D}}(Re) = C_{\text{D}}(Re_\infty)[f_1(\varepsilon)f_2(\vartheta)]^{-2} \quad (11)$$

The drag coefficient for the isolated bubble was calculated using Karamanev's correlation [31], whilst the shape factor was estimated utilising the correlation of Vakrushev and Efremov recommended by Clift et al. [32]. The correction factor for the population effect varied according to the bubbling regime. For the homogeneous regime, the expression developed by Behringer [33] was used on account of its agreement with experimental data from different authors [34–37]. On the other hand, for the heterogeneous regime, when $Eo > 40$, the relation proposed by Krishna et al. [38] was utilised, whereas, if $Eo \leqslant 40$, the correction factor was assumed unitary, since no correlation for its estimation was found in the literature. Hence:

$$f_1 = \begin{cases} 1-\varepsilon & \text{if } u_{\text{G}} \leqslant u_{\text{trans}} \\ 1 & \text{if } u_{\text{G}} > u_{\text{trans}} \text{ and } Eo \leqslant 40 \\ 2.73 + 4.505(u_{\text{G}} - u_{\text{trans}}) & \\ & \text{if } u_{\text{G}} > u_{\text{trans}} \text{ and } Eo > 40 \end{cases} \quad (12)$$

With regard to the correction for the wall effect, for $Eo < 40$, its value was calculated using the heuristic formula presented by Clift et al. [32], while the relation of Collins [39] was adopted for $Eo \geqslant 40$, both of which were shown to agree well with the experimental data of Krishna et al. [40]. The parameter f_2^*, related to the possibility of neglecting the wall effect, was evaluated according to Clift et al. [32].

$$f_2^* = \begin{cases} 1 & \text{if } Eo < 40 \text{ and } \vartheta \leqslant 0.06 \text{ and } Re \leqslant 0.1 \\ 1 & \text{if } Eo < 40 \text{ and } \vartheta \leqslant 0.08 + 0.02\log_{10} Re \\ & \quad \text{and } 0.1 \leqslant Re \leqslant 100 \\ 1 & \text{if } Eo < 40 \text{ and } \vartheta \leqslant 0.12 \text{ and } Re > 100 \\ 1 & \text{if } Eo \geqslant 40 \text{ and } \vartheta < 0.125 \\ 0 & \text{otherwise} \end{cases} \quad (13a)$$

$$f_2 = \begin{cases} 1 & \text{if } f_2^* = 1 \\ (1-\vartheta^2)^{3/2} & \text{if } Eo < 40 \text{ and } f_2^* = 0 \\ 1.13e^{-\vartheta} & \text{if } Eo \geqslant 40 \text{ and } 0.125 \leqslant \vartheta \leqslant 0.6 \\ 0.62\vartheta^{-1/2} & \text{if } Eo \geqslant 40 \text{ and } \vartheta > 0.6 \end{cases} \quad (13b)$$

At the end of the ascension stage, the total mass of vaporised liquid, m_{ev}, and the total amount of sensible heat transferred to the liquid, q_{s}, associated with each kind of bubble are evaluated. For the 'small' bubbles, as there is no identity loss in the transition from formation to ascension, Eq. (4a) and the definition of h_{ext} are used to give:

$$m_{\text{ev}}^{\text{sb}} = 4\pi\int_0^{t_{\text{res}}} R^2\rho_{\text{G}_{\text{sur}}}\left(v_{\text{sur}} - \frac{\mathrm{d}R}{\mathrm{d}t}\right)\mathrm{d}t \quad (14)$$

$$q_{\text{s}}^{\text{sb}} = 4\pi\int_0^{t_{\text{res}}} R^2h_{\text{ext}}(T_{\text{sur}} - T_{\text{L}})\,\mathrm{d}t \quad (15)$$

where $t_{res} = t_{form} + t_{asc}$.

As regards the 'large' bubbles, the preceding integration has to be divided into the terms related to the formation and ascension stages, since the coalescence process leads to a change in the calculation basis used for each stage. From a mass balance, the number n_{sb} of 'small' bubbles needed to originate, by coalescence, one 'large' bubble equals $n_{sb} = (m_{lb,form}/m_{sb,form}) = (R_{exp}/R_{form})^3(\bar{\rho}_{G,asc,lb}/\bar{\rho}_{G,form,sb})$, where $\bar{\rho}_{G,asc,lb} = \rho_G(T(r,0)|_{asc,lb}, Y_1(r,0)|_{asc,lb})$ (see Eqs. (8b) and (8c)) and $\bar{\rho}_{G,form,sb}$ is the mean density of the small bubble at the end of its formation. As a result, the quantities associated with the 'large' bubble are

$$m_{ev}^{lb} = 4\pi\left[n_{sb}\int_0^{t_{form}} R^2\rho_{G_{sur}}\left(v_{sur} - \frac{dR}{dt}\right)dt + \int_{t_{form}}^{t_{asc}} R^2\rho_{G_{sur}}\left(v_{sur} - \frac{dR}{dt}\right)dt\right] \quad (16)$$

$$q_s^{lb} = 4\pi\left[n_{sb}\int_0^{t_{form}} R^2 h_{ext}(T_{sur} - T_L)\,dt + \int_{t_{form}}^{t_{asc}} R^2 h_{ext}(T_{sur} - T_L)\,dt\right] \quad (17)$$

2.2. Continuous phase model

A schematic representation of the direct-contact evaporator considered in this work is presented in Fig. 1b, in which the mass and heat-transfer rates are evidenced. Apart from the feed (M_{feed}), outlet (M_{out}) and evaporate (M_{ev}) streams, there is the condensate stream coming from the column freeboard (M_{cond}) due to heat losses from the outlet stream to the surroundings. As for the heat-transfer rates, not only the superheated gas (Q_s) but also the sparger (Q_d) provides energy for the liquid, part of which is inevitably lost to the surroundings (Q_p).

Assuming the liquid to be perfectly mixed due to the vigorous bubbling-driven mixing, which has already been experimentally verified by different authors [5,6,41,42], and the entrainment of liquid in the gas phase to be negligible, the following mass and heat balances can be written for the continuous phase:

$$\frac{dm_L}{dt} = M_{feed} + M_{cond} - M_{ev} - M_{out} \quad (18)$$

$$\frac{d(m_L X_L)}{dt} = M_{feed}X_{feed} - M_{out}X_L \quad (19)$$

$$\frac{d[m_L Cp_L(T_L - T_{feed})]}{dt} = Q_s + Q_d - Q_p + M_{cond}Cp_L^0(T_{ev} - T_{feed}) - M_{ev}\widetilde{C}p_L(T_L - T_{feed}) - M_{out}Cp_L(T_L - T_{feed}) \quad (20)$$

in which the feed temperature is adopted as reference for enthalpy calculation and the variables Cp_L, Cp_L^0 and $\widetilde{C}p_L$ are, respectively, the heat capacity of the solution, the heat capacity of the pure solvent and the partial mass heat capacity of the solvent in the solution. Substitution of Eq. (18) into Eq. (19) gives:

$$m_L\frac{dX_L}{dt} = M_{feed}(X_{feed} - X_L) + (M_{ev} - M_{cond})X_L \quad (21)$$

Considering the heat capacity of the continuous phase to be constant and equal to the value associated with the pure solvent ($Cp_L = Cp_L^0$, hence $\widetilde{C}p_L = Cp_L^0$) and using Eq. (18), Eq. (20) may be rewritten as:

$$m_L Cp_L\frac{dT_L}{dt} = Q_s + Q_d - Q_p + M_{cond}Cp_L(T_{ev} - T_L) - M_{feed}Cp_L(T_L - T_{feed}) \quad (22)$$

an expression which is only valid for dilute solutions or pure liquids, since the hypothesis of a heat capacity independent of solute concentration clearly does not hold for concentrated solutions. In the calculation of both Q_d and Q_p the corresponding overall heat-transfer coefficients, U_d and U_p, are used, both of which constitute input parameters of the model and should, therefore, be estimated or experimentally determined.

The evaporation and sensible heat-transfer rates are evaluated based on the weighting of the results for the two kinds of bubbles obtained with the dispersed phase model. In this model, the mass of vaporised liquid per bubble, the amount of sensible heat transferred per bubble and the frequency of bubble formation at the orifices are all calculated, so that, knowing the number of orifices in the sparger, N_o, one may compute the evaporation and sensible heat-transfer rates associated with each kind of bubble. For the 'small' bubbles, for instance, we have:

$$M_{ev,sb} = N_o f_o^{sb} m_{ev}^{sb}, \quad Q_{s,sb} = N_o f_o^{sb} q_s^{sb} \quad (23)$$

In the homogeneous regime, since one single bubble size is admitted, Eq. (23) already gives the values related to the dispersed phase, as done by Campos and Lage [10] in their model. Nevertheless, in the heterogeneous regime, the effective contribution of each kind of bubble has to be taken into account. The 'large' bubbles derive from coalescence phenomena, whose extension grows with the gas flow rate. In addition, the formation of these bubbles only commences when the homogeneous regime becomes unstable, that is, when the gas superficial velocity, u_G, exceeds its transition value, u_{trans}. These two facts are consistent with weighting the data in terms of the fraction of the gas superficial velocity which surpasses u_{trans}, a criterion which has already been used in the elaboration of gas hold-up models for the heterogeneous regime [12–15,43]. Thus, the rates M_{ev} and Q_s are given by the following relations:

$$M_{ev} = N_o u_G^{-1}\left[f_o^{sb} m_{ev}^{sb} u_{trans} + f_o^{lb} m_{ev}^{lb}(u_G - u_{trans})\right] \quad (24)$$

$$Q_s = N_o u_G^{-1}\left[f_o^{sb} q_s^{sb} u_{trans} + f_o^{lb} q_s^{lb}(u_G - u_{trans})\right] \quad (25)$$

where $f_o^{sb} = 1/t_{form}$ and $f_o^{lb} = f_o^{sb}/n_{sb}$. No relation was found in the literature for estimating the transition velocity in direct-contact evaporators. As a result, the prediction of the regime transition point was based on the correlation developed by Reilly et al. [44] for isothermal bubble columns, whose adequacy for pure liquids has been recently confirmed by Krishna et al. [45].

With the aim of estimating the condensing rate in the upper region of the equipment, it is assumed that only latent heat is lost and, therefore, the condensate temperature remains equal to the evaporate one and the condensation rate is equal to $M_{cond} = Q_p^{fb}/\Delta H_{vap}(T_{ev})$, where Q_p^{fb} is the heat-transfer rate from the outlet gas stream to the surroundings in the freeboard region of the evaporator. The Q_p^{fb} value was estimated assuming unidimensional, steady-state heat transfer and considering the conduction resistances of the evaporator wall and insulating layer, as well as the resistance associated with free convection to the surroundings:

$$Q_p^{fb} = \frac{2\pi(H_c - H_b)(T_{ev} - T_{amb})}{\lambda_c^{-1}\ln(D_e/D_c) + \lambda_{isl}^{-1}\ln(D_{isl}/D_e) + (D_{isl}h_{amb})^{-1}} \quad (26)$$

In Eq. (26) the ambient convective heat-transfer coefficient, h_{amb}, was computed using the relation recommended by Kreith [46] for laminar free convection outside cylindrical vertical ducts.

2.3. Gas hold-up

The prediction of the overall height of the two-phase mixture, a key parameter in the simulation of a direct-contact evaporator, requires the determination of the gas hold-up in the unit. Even though a vast number of correlations for predicting the gas hold-up in isothermal bubble columns has already been published, a revision of which may be found in the works of Shah et al. [47] and Saxena and Rao [48], these correlations fail considerably when applied to direct-contact evaporators, as shown by Queiroz [5]. For the homogenous bubbling regime, Campos and Lage [27,28] presented a general correction factor for these relations which accounted for heat and mass transfer effects and enabled their application for non-isothermal bubbling. Thus, completing the evaporator model, an expression for this correction factor in the heterogeneous regime is proposed in this section.

Starting from the gas hold-up definition, the gas and liquid volumes in the mixture are related by $(V_G/V_L) = \varepsilon(1-\varepsilon)^{-1}$ which, for the model with two bubble sizes, may be divided into two terms:

$$(V_G^{sb}/V_L) = \varepsilon_{sb}(1-\varepsilon)^{-1}, \quad (V_G^{lb}/V_L) = \varepsilon_{lb}(1-\varepsilon)^{-1} \quad (27)$$

The total gas volume is a function of the number of orifices in the spargers, the mean volume of the bubbles in each class, their frequency of formation and their residence time, being the last three influenced by heat and mass transfer processes, which justifies the gas hold-up differences between isothermal and non-isothermal bubbling. The gas volume associated with each kind of bubble is given by

$$V_G^{sb} = N_o\overline{V_{sb}}f_o^{sb}t_{res}^{sb}, \quad V_G^{lb} = N_o\overline{V_{lb}}f_o^{lb}t_{res}^{lb} \quad (28)$$

In view of the fact that the available correlations for ε refer to isothermal processes, a hypothetical bubbling process is considered, in which the liquid volume and the temperatures of both phases are identical to the ones related to the real process, but neither heat nor mass transfer occurs. Upon applying Eq. (27) to these two processes and computing, for each kind of bubble, the ratio between the obtained relations, one gets:

$$\frac{\varepsilon_{sb}}{1-\varepsilon} = \frac{V_G^{sb}}{(V_G^{sb})_{hyp}}\left(\frac{\varepsilon_{sb}}{1-\varepsilon}\right)_{hyp}$$
$$\frac{\varepsilon_{lb}}{1-\varepsilon} = \frac{V_G^{lb}}{(V_G^{lb})_{hyp}}\left(\frac{\varepsilon_{lb}}{1-\varepsilon}\right)_{hyp} \quad (29)$$

where the subscript hyp refers to hypothetical bubbling. The sum of the two relations given by Eq. (29) yields a relation between the gas hold-up for the real and hypothetical processes:

$$\frac{\varepsilon}{1-\varepsilon} = \frac{V_G^{sb}}{(V_G^{sb})_{hyp}}\left(\frac{\varepsilon_{sb}}{1-\varepsilon}\right)_{hyp} + \frac{V_G^{lb}}{(V_G^{lb})_{hyp}}\left(\frac{\varepsilon_{lb}}{1-\varepsilon}\right)_{hyp} \quad (30)$$

The application of Eq. (30) is restricted to that limited fraction of the available isothermal correlations for which the gas hold-up is divided into terms associated with the two kinds of bubbles. However, defining ψ as the ratio between the real and hypothetical gas volumes, Eq. (30) can be rewritten in the following form:

$$\frac{\varepsilon}{1-\varepsilon} = \frac{\psi_{sb}(\varepsilon_{sb})_{hyp} + \psi_{lb}(\varepsilon_{lb})_{hyp}}{(\varepsilon_{sb} + \varepsilon_{lb})_{hyp}}\left(\frac{\varepsilon}{1-\varepsilon}\right)_{hyp} \quad (31)$$

With Eq. (31), given a model for the isothermal gas hold-up which distinguishes the contributions of 'small' and 'large' bubbles, any gas hold-up correlation for isothermal bubbling can be tested for calculating the gas hold-up in a direct-contact evaporator operating in the heterogeneous regime. Thus, Eq. (31) constitutes the expansion, to heterogeneous regime, of the correction factor proposed by Campos and Lage [27,28].

The ratio ψ is calculated by applying Eq. (28) to 'small' and 'large' bubbles, respectively, considering the real and hypothetical bubbling processes. For the hypothetical process, since there is no heat and mass transfer, the parameters $\overline{V_b}$, f_o and t_{res} are computed with the solution of the dynamic models for the formation

(Eq. (6)) and ascension (Eq. (9)) stages, whereas, for the real process, these parameters are given by the model of the dispersed phase. In the case of the 'small' bubbles, the relation developed by Campos and Lage [28] applies:

$$\psi_{sb} = \frac{(\overline{R_{res}})^3 f_o^{sb} t_{res}^{sb}}{\left[(\overline{R_{res}})^3 f_o^{sb} t_{res}^{sb}\right]_{hyp}} \tag{32}$$

On the other hand, for the 'large' bubbles, the contributions of the formation and ascension stages have to be calculated separately:

$$\psi_{lb} = \frac{(\overline{R_{form}})^3 f_o^{sb} t_{form}^{sb} + f_o^{lb}(\overline{R_{asc}})^3 t_{asc}^{lb}}{\left[(\overline{R_{form}})^3 f_o^{sb} t_{form}^{sb} + f_o^{lb}(R_{exp})^3 t_{asc}^{lb}\right]_{hyp}} = \frac{(\overline{R_{form}})^3 + f_o^{lb}(\overline{R_{asc}})^3 t_{asc}^{lb}}{\left[(\overline{R_{form}})^3 + f_o^{lb}(R_{exp})^3 t_{asc}^{lb}\right]_{hyp}} \tag{33}$$

3. Numerical procedure

As detailed by Campos and Lage [27,28], the dispersed phase model was written in a dimensionless form and then solved by the method of lines using finite-volume spatial discretisation. Eqs. (18), (21) and (22), which comprise the continuous phase model, were integrated using the DDASPG routine from the IMSL library. During this integration, the dispersed phase model periodically updates the values of Q_s, M_{ev} and ε. In the case of ε, the contributions of 'small' and 'large' bubbles for the isothermal gas hold-up in Eq. (31) were evaluated utilising the model of Ellenberger and Krishna [14]. The calculation parameters of the dispersed phase model, such as number of discretization points, time integration tolerance and number of quadrature points in the determination of Q_s and M_{ev}, were varied to assure that convergence was obtained in the results. The results discussed herein were determined with a degree of accuracy higher than 0.1%.

The model was tested against experimental data for the air–water system. To perform the simulations, air and steam physical properties, as well as water viscosity and water latent heat of vaporisation, were estimated using the correlations of Lage [49]. The equation presented by Reid et al. [50] was employed in the estimation of water vapour pressure, being the data given by Holman [51] used for the other necessary water properties. For the lower gas superficial velocity, at which the unit operates in the homogeneous bubbling regime, the isothermal gas hold-up was calculated utilising the correlation of Luo et al. [52], whereas, for the other values of u_G, the correlation of Ellenberger and Krishna [14], developed for the heterogeneous regime, was applied.

4. Results and discussion

The validity of the proposed model for dynamic simulation of direct-contact evaporators was assessed by means of a comparison between its predictions and some of the experimental data reported by Ribeiro and Lage [3] for the air–water system in semi-batch operation. Following Campos and Lage [10] procedure, the thermal capacitance of the evaporator (8.80×10^3 J K^{-1}) was added to the liquid-phase thermal capacitance in Eq. (22) for taking into account, in a simplified manner, the thermal inertia of the evaporator. The overall heat-transfer coefficients used in the simulation were determined based upon the experimental heat-transfer rates reported by Ribeiro and Lage [3]. The U_d values with their 95% confidence intervals were calculated as (10.1 ± 0.3), (17.7 ± 0.4), (19.0 ± 0.6) and (21.4 ± 1.2) W m^{-2} K^{-1} for $u_G = 2.2$, 4.4, 6.6 and 12.1 cm/s, respectively. As U_p does not depend upon the gas superficial velocity, the value determined for $u_G = 6.6$ cm/s, namely (1.6 ± 0.2) W m^{-2} K^{-1}, was used for all simulations. The 'large' bubble radii at the beginning of the ascension stage, R_{exp}, were taken as the experimental 'large' bubble radii in the column reported by of Ribeiro and Lage [53], being 5.3, 7.5 and 8.0 mm, for $u_G = 4.4$, 6.6 and 12.1 cm/s, respectively. For $u_G = 2.2$ cm/s, there is only the 'small' bubble class.

For the perforated plate sparger analysed by Ribeiro and Lage [3], the predicted values of liquid temperature, bubbling height and evaporation rate are compared with experimental data in Figs. 2–5. Also included in these figures are the results of the model elaborated by Campos and Lage [10] for operation in the homogenous bubbling regime.

In the specific case of the lower gas superficial velocity, as the evaporator operates in the homogeneous regime, both models provide the same results, for the proposed equations constitute an extension to the heterogeneous regime of the original formulation of Campos and Lage [10]. An excellent agreement between experimental data and simulation results for both bubbling height and evaporation rate is exhibited in Fig. 2. With regard to the liquid temperature, the deviations are somewhat higher but still quite satisfactory, confirming, thus, the adequacy of the model of Campos and Lage [10] for an evaporator operating in the homogeneous bubbling regime.

However, differences between the predictions of the two models arise when the other gas superficial velocities are considered. These differences are small as far as the liquid temperature is concerned, with both models giving results consonant with the experimental data. As regards the bubbling height, the discrepancies between the models increase a little but are still in the range of the experimental error associated with this variable. In fact, the main distinctions are related to the evaporation rate.

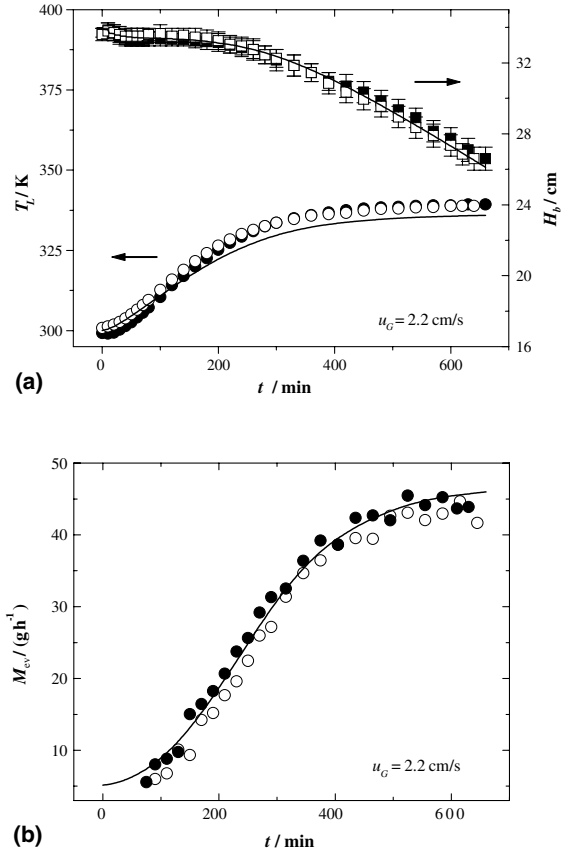

Fig. 2. Comparison between simulation results (lines) and experimental data [3] (symbols) for the direct-contact evaporator operating with $u_G = 2.2$ cm/s and the perforated plate: (a) liquid temperature and bubbling height; (b) evaporation rate.

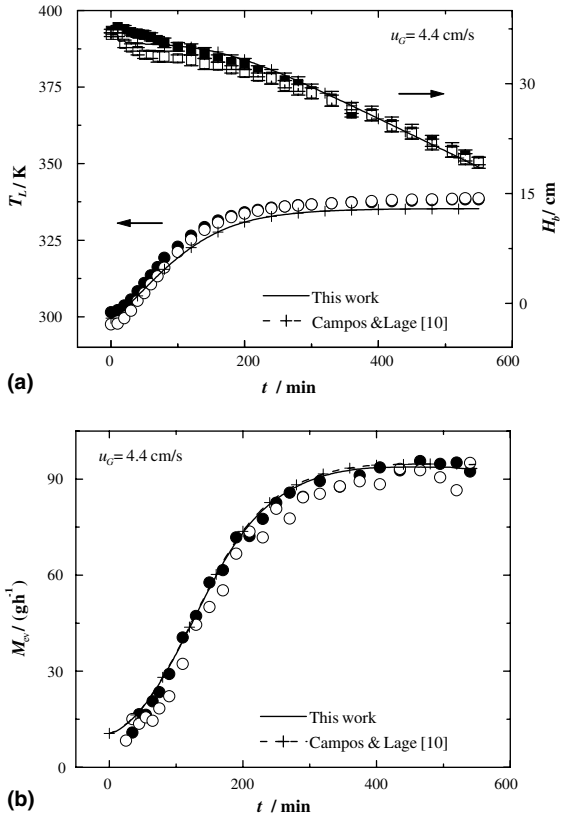

Fig. 3. Comparison between experimental data [3] (symbols) for $u_G = 4.4$ cm/s and simulation results (lines) given by two distinct models, the one proposed in this work and the one of Campos and Lage [10]: (a) liquid temperature and bubbling height; (b) evaporation rate.

Initially, for $u_G = 4.4$ cm/s, since operation takes place at the beginning of the regime transition region and the fraction of 'large' bubbles in the mixture is small, the evaporation rate obtained with the proposed model is only slightly smaller than the one predicted by the homogeneous regime model, and both predictions seem to represent the experimental data well. Nonetheless, as u_G increases, the contribution of the 'large' bubbles grows, so that the evaporation rate curves for the two models become progressively different. From Figs. 4b and 5b it is clear that, for the higher gas superficial velocities, the quasi-steady-state evaporation rates predicted by the model of Campos and Lage [10] exceed the experimental ones, whereas, with the proposed model, values in better agreement with the experimental data are obtained. Being the evaporation rate an essential parameter of any evaporator, these results demonstrate that the proposed model is more appropriate for representing the operation in the heterogeneous bubbling regime. By neglecting coalescence effects in the ascension stage, the model of Campos and Lage [10] considers a greater interfacial area and, at the same time, a greater residence time, both of which favours mass transfer from the liquid phase to the bubble, which justifies the higher evaporation rates predicted by this model.

In order to complete the model validation, the adequacy of the correction factor for the gas hold-up was evaluated. Fig. 6 presents a comparison of the experimental data for the perforated plate sparger [3] with both the values predicted with Eq. (31) and the ones given by the isothermal correlations considered in this work. For the sake of clarity, the error bars are only shown for one data set for each u_G value.

Regardless of the gas superficial velocity, there is always an increase in the gas hold-up at the very beginning of the operation, followed by a decrease, after which an equilibrium value is reached in the quasi-steady-state regime. According to the results in Fig. 6, neither this dynamic behaviour nor the quasi-steady-state value is well represented by the employed gas

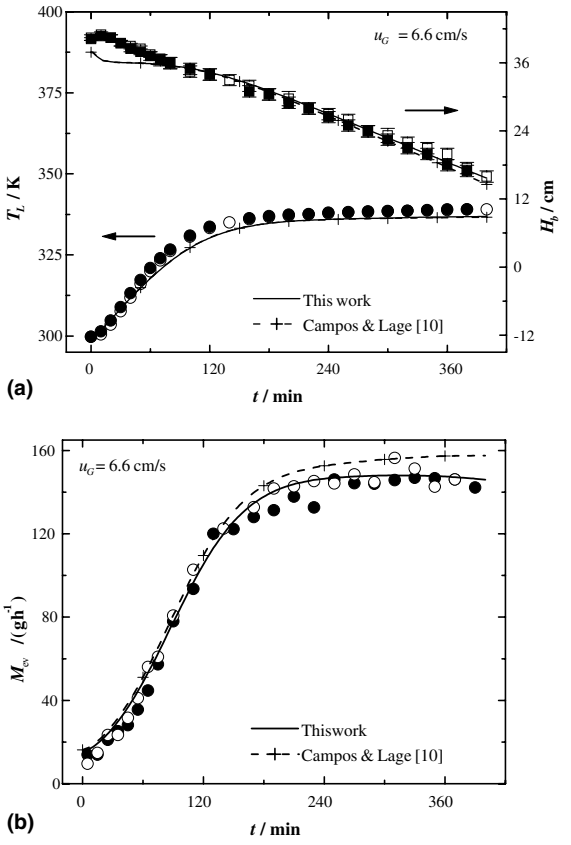

Fig. 4. Comparison between experimental data [3] (symbols) for $u_G = 6.6$ cm/s and simulation results (lines) given by two distinct models, the one proposed in this work and the one of Campos and Lage [10]: (a) liquid temperature and bubbling height; (b) evaporation rate.

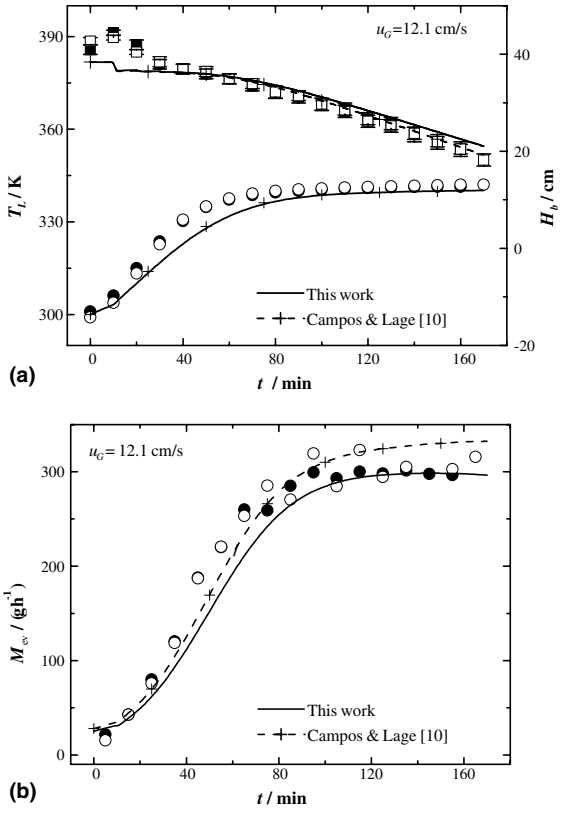

Fig. 5. Comparison between experimental data [3] (symbols) for $u_G = 12.1$ cm/s and simulation results (lines) given by two distinct models, the one proposed in this work and the one of Campos and Lage [10]: (a) liquid temperature and bubbling height; (b) evaporation rate.

hold-up isothermal correlations. With the application of the correction factor for non-isothermal bubbling, a substantial improvement in the prediction of the gas hold-up quasi-steady-state value is observed, demonstrating, thus, the adequacy of Eq. (31). For the lowest gas superficial velocity, even the gas hold-up dynamic behaviour seems to be well predicted, whereas, in the other cases, the prediction of the dynamic behaviour remains unsuccessful. The correction factor was less than 1 for all gas superficial velocities, indicating that the shrinking effect due to the significant drop in the gas temperature outweighs the mass increase due to vaporisation, which is consonant with the findings of Moody [8] and Campos and Lage [27].

As previously discussed by Ribeiro and Lage [3], the initial gas-hold increase observed in Fig. 6a–d might be related to the establishment of the liquid circulation pattern in the column. Since gas hold-up correlations are developed using data from columns whose liquid circulation pattern is already established, it is natural that such correlations do not enable one to predict this initial increase.

As regards the region of gas hold-up decrease, Ribeiro and Lage [3] have demonstrated that its occurrence is associated with the evolution of bubble coalescence and breakage phenomena and the resulting temporal change of the bubble size distribution which is brought about by the augmentation of the liquid temperature. Therefore, the accurate calculation of the gas hold-up dynamic behaviour in a direct-contact evaporator will require the knowledge of the temporal evolution of the bubble size distribution in the equipment.

Apart from the perforated plate, Ribeiro and Lage [3] have also reported experimental data for a porous plate sparger. In the case of this distributor, the only bubble formation model available in the literature, namely the one proposed by Bowonder and Kumar [54], predicted bubble formation diameters much smaller than the experimental volumetric mean bubble diameters deter-

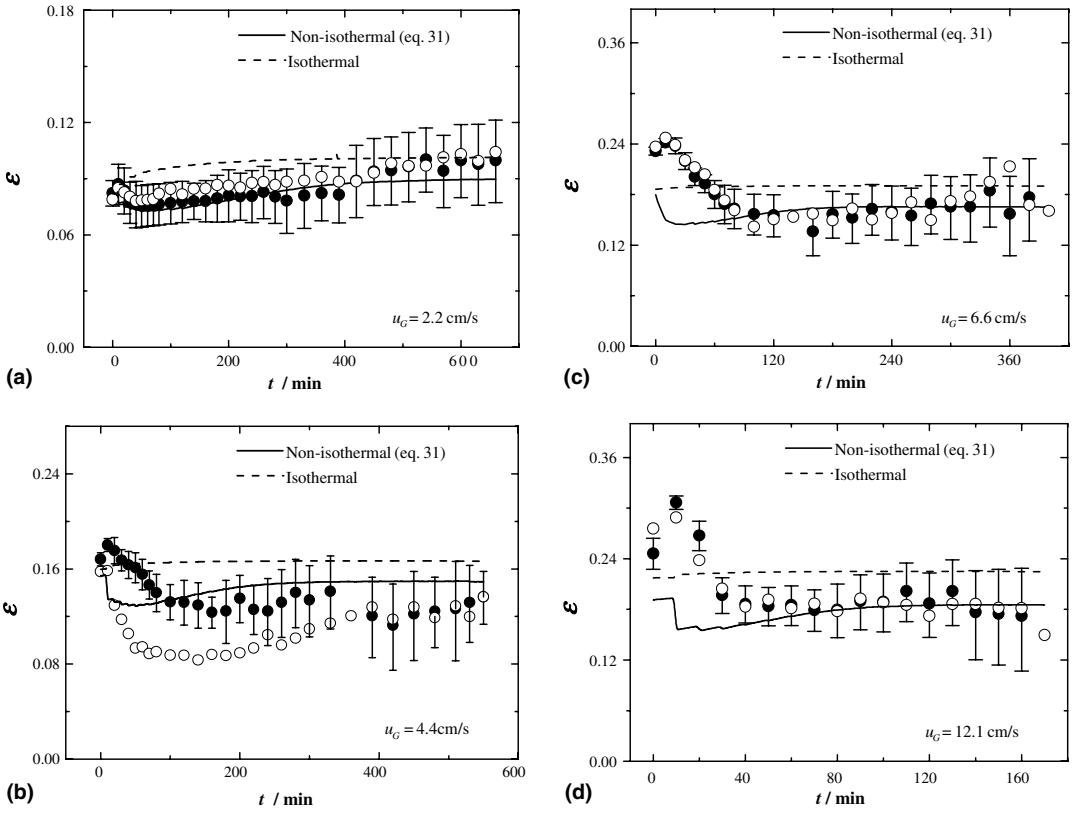

Fig. 6. Comparison between experimental gas hold-up [3] (symbols) and the values (lines) calculated with the isothermal correlations considered with and without the non-isothermal bubbling correction proposed.

mined by Ribeiro and Lage [3], which was attributed to coalescence at the formation stage. Therefore, the formal application of the developed evaporator model for the case of the porous plate sparger would require a new bubble formation model. As a simpler alternative, it was decided to specify the bubble diameter at the end of the formation stage and then verify whether or not the model would provide good estimates of the evaporator performance.

Thus, for simulating the evaporator with the porous plate as sparger, the Davidson and Schüler [30] model for bubble formation was maintained, being the experimental volumetric mean bubble radius at the quasi-steady conditions specified as the detachment criterion. The number of effective orifices in the porous plate was calculated according to the assumption of a close hexagonal packed arrangement of the formed bubbles, adopted in the original Bowonder and Kumar's formulation [54]. Since the bubble formation diameter for the isothermal process was not calculated, the correction factor for gas hold-up could not be estimated, and the prediction of an isothermal correlation had to be directly employed. In view of the fact that bubble interaction phenomena during the ascension stage eliminate the sparger effect for the high gas superficial velocities [3], simulation was only performed for $u_G = 2.2$ cm/s. In this case, the gas hold-up correlation of Luo et al. [52], developed for perforated plates, was substituted by the one presented by Sotelo et al. [55] for porous plates, being all gas properties evaluated at the liquid temperature. Also, the heat-transfer coefficient for the porous plate sparger had the larger value of (11.7 ± 0.5) W/m^2 K. The obtained results are compared with experimental data in Fig. 7.

As far as the evaporation rate and the liquid temperature are concerned, the predictions of the evaporator model are in good agreement with the experimental data, corroborating, therefore, the adequacy of the heat and mass transfer modelling. The dynamic gas hold-up behaviour, shown by Ribeiro and Lage [3] to be related to a temporal variation of the bubble size distribution, is not well represented, as such effect was not considered in the development of the used isothermal correlation. These differences are reproduced in the bubbling height curve. The quasi-steady-state gas hold-up, however, is consonant with the experimental measurements.

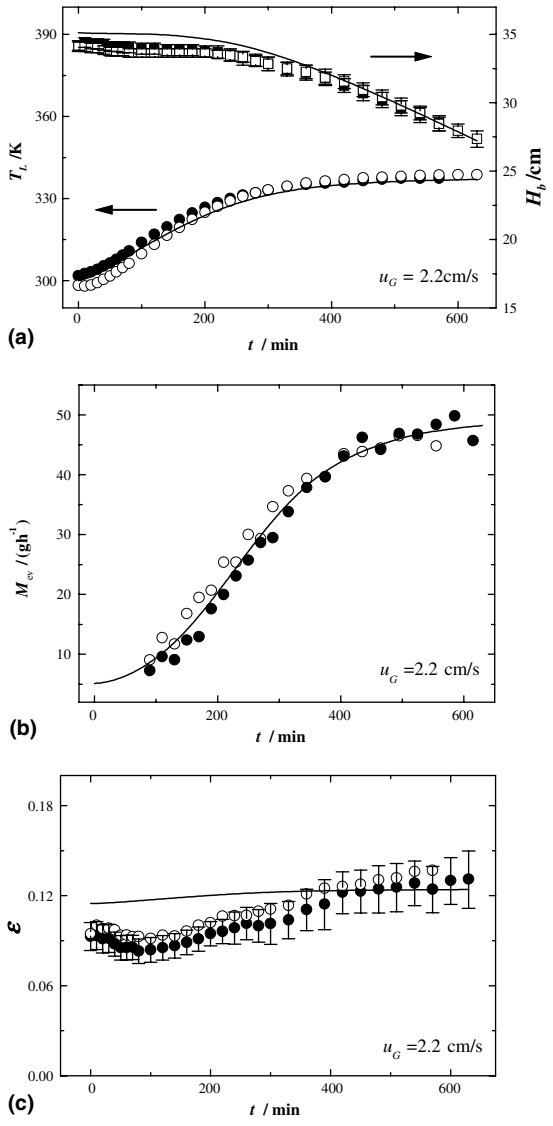

Fig. 7. Comparison between simulation results (lines) and experimental data [3] (symbols) for the direct-contact evaporator operating with $u_G = 2.2$ cm/s and the porous plate: (a) liquid temperature and bubbling height; (b) evaporation rate; (c) gas hold-up.

5. Conclusions

A two-bubble class model for the dynamic simulation of direct-contact evaporators operating in the heterogeneous bubbling regime was proposed. Its predictions of evaporation rate, bubbling height and liquid temperature transient profiles were shown to be in good agreement with the experimental data for the air–water system reported by Ribeiro and Lage [3] for four different values of gas superficial velocity using a perforated plate sparger.

As a part of this model, a general correction factor due to heat and mass transfer effects was developed for isothermal gas hold-up correlations in order to enable their application to direct-contact evaporators operating in the heterogeneous regime. Comparison with experimental data confirmed the inadequacy of the isothermal gas hold-up correlations and demonstrated the adequacy of the proposed correction factor, whose application led to a good prediction of the gas hold-up quasi-steady-state value for all gas superficial velocities considered by Ribeiro and Lage [3].

The proposed model with an experimental mean bubble size was also capable of simulating the experimental data for the air–water system in the homogeneous bubbling regime reported by Ribeiro and Lage [3] for a porous plate sparger.

Acknowledgements

The authors would like to thank CNPq (grant no. 550614/02-8) and FAPERJ (E-26/170.420/99-APQ1) for the financial support provided.

References

[1] C.S. Cronan, Submerged combustion flares anew, Chem. Eng. 63 (2) (1956) 163–167.
[2] A. Williams, Submerged combustion for water plants, Mech. Eng. 87 (7) (1965) 34–37.
[3] C.P. Ribeiro Jr., P.L.C. Lage, Direct-contact evaporation in the homogeneous and heterogeneous bubbling regime. Part I: Experimental analysis, Int. J. Heat Mass Transfer, in press.
[4] A.L. Andrade, Heat transfer in superheated bubbles, DSc thesis, PEQ/COPPE/UFRJ, Rio de Janeiro, RJ, 1985 (in Portuguese).
[5] E.M. Queiroz, Simultaneous heat and mass transfer in bubbling processes, DSc thesis, PEQ/COPPE/UFRJ, Rio de Janeiro, RJ, 1990 (in Portuguese).
[6] C. Guy, P.J. Carreau, J. Paris, Heat and mass transfer between bubbles and a liquid, Can. J. Chem. Eng. 70 (1) (1992) 55–60.
[7] P.L.C. Lage, C.M. Hackenberg, Simulation and design of direct-contact evaporators, in: T.N. Veziroglu (Ed.), Multiphase Transport Particulate Phenomena, vol. 2, Hemisphere Publishing Corporation, New York, 1990, pp. 577–592.
[8] F.J. Moody, Dynamic and thermal behavior of hot gas bubbles discharged into water, Nucl. Eng. Des. 95 (1986) 47–54.
[9] S.V. Komarov, M. Sano, Bubble behaviour and heat transfer in preheated gas injection into liquid bath, ISIJ Int. 38 (10) (1998) 1045–1052.
[10] F.B. Campos, P.L.C. Lage, Modelling and simulation of direct-contact evaporators, Braz. J. Chem. Eng. 18 (3) (2001) 277–286.

[11] D.J. Vermeer, R. Krishna, Hydrodynamics and mass transfer in bubble columns operating in the churn-turbulent regime, Ind. Eng. Chem. Process Des. Develop. 20 (1981) 475–482.
[12] R. Krishna, P.M. Wilkinson, L.L. Van Dierendonck, A model for gas holdup in bubble columns incorporating the influence of gas density on flow regime transitions, Chem. Eng. Sci. 46 (10) (1991) 2491–2496.
[13] P.M. Wilkinson, A.P. Spek, L.L. Van Dierendonck, Design parameters estimation for scale-up of high-pressure bubble columns, AIChE J. 38 (4) (1992) 544–554.
[14] J. Ellenberger, R. Krishna, A unified approach to the scale-up of gas–solid fluidised bed and gas–liquid bubble column reactors, Chem. Eng. Sci. 49 (24B) (1994) 5391–5411.
[15] H.M. Letzel, J.C. Schouten, R. Krishna, C.M. Van Den Bleek, Gas holdup and mass transfer in bubble column reactors operated at elevated pressure, Chem. Eng. Sci. 54 (1999) 2237–2246.
[16] M. Iguchi, Z. Morita, H. Tokunaga, H. Tatemichi, Heat transfer between bubbles and liquid during cold gas injection, ISIJ Int. 32 (7) (1992) 865–872.
[17] H. Tokunaga, M. Iguchi, H. Tatemichi, Heat transfer between bubbles and molten wood's metal, ISIJ Int. 35 (1) (1995) 21–25.
[18] P. Grassmann, E. Wyss, Determination of heat and mass transfer coefficients between steam bubbles and fluids, Chem. Ing. Tech. 34 (11) (1962) 755–759 (in German).
[19] S.S. Bhagade, J.R. Giradkar, P.S. Mene, Studies on heat transfer during bubble formation, Indian J. Technol. 11 (7) (1973) 281–283.
[20] A.I. Safonov, K.V. Gomonova, V.S. Krylov, Heat transfer to a growing bubble during gas dispersion in a liquid, Theor. Found. Chem. Eng. 8 (5) (1975) 654–660.
[21] A. Jeje, B. Ross, The temperature field near a nozzle and the dynamics of saturated steam bubbles in subcooled water at low steady vapor supply rates, Chem. Eng. Sci. 43 (10) (1988) 2817–2831.
[22] A.D. Pinto, Bubble formation at orifices: initial evaporation in bubbling processes, MSc dissertation, PEQ/COPPE/UFRJ, Rio de Janeiro, RJ, 1990 (in Portuguese).
[23] S.C. Cho, W.K. Lee, Steam bubble formation at a submerged orifice in quiescent water, Chem. Eng. Sci. 46 (3) (1991) 789–795.
[24] A.C. Mezavilla, Direct-contact evaporation: heat and mass transfer during the formation of superheated bubbles, MSc dissertation, PEQ/COPPE/UFRJ, Rio de Janeiro, RJ, 1995 (in Portuguese).
[25] C.M. Hackenberg, Heat transfer in bubbles, MSc dissertation, PEQ/COPPE/UFRJ, Rio de Janeiro, RJ, 1965 (in Portuguese).
[26] R.I. Nigmatulin, N.S. Khabeev, F.B. Nagiev, Dynamics, heat and mass transfer of vapour–gas bubbles in a liquid, Int. J. Heat Mass Transfer 24 (6) (1981) 1033–1044.
[27] F.B. Campos, P.L.C. Lage, Simultaneous heat and mass transfer during the ascension of superheated bubbles, Int. J. Heat Mass Transfer 43 (2) (2000) 179–189.
[28] F.B. Campos, P.L.C. Lage, Heat and mass transfer modelling during the formation and ascension of superheated bubbles, Int. J. Heat Mass Transfer 43 (16) (2000) 2883–2894.
[29] P.H. Calderbank, M.B. Moo-Young, The continuous phase heat and mass-transfer properties of dispersions, Chem. Eng. Sci. 16 (1–2) (1961) 39–54.
[30] J.F. Davidson, B.O.G. Schüler, Bubble formation at an orifice in a viscous liquid, Trans. Inst. Chem. Eng. 38 (1960) 144–154.
[31] D.G. Karamanev, Rise of gas bubbles in quiescent liquids, AIChE J. 40 (8) (1994) 1418–1421.
[32] R. Clift, J.R. Grace, M.W. Weber, Bubbles, Drops and Particles, Academic Press, New York, 1978, pp. 181–182, 232–236.
[33] H. Behringer, The flow of liquid-gas mixtures in vertical tubes, Z. Ges. Kälte-Ind. 43 (1936) 55–58.
[34] N. Zuber, J.A. Findlay, Average volumetric concentration in two-phase flow systems, J. Heat Transfer 87 (4) (1965) 453–468.
[35] D. Bhaga, M.E. Weber, Hold-up in vertical two and three phase flow, Can. J. Chem. Eng. 50 (2) (1972) 323–336.
[36] J.H. Hills, R.C. Darton, The rising velocity of a large bubble in a bubble swarm, Trans. Inst. Chem. Eng. 54 (4) (1976) 258–264.
[37] J. Zahradnik, M. Fialova, M. Ruzicka, J. Drahos, F. Kastanek, N.H. Thomas, Duality of the gas–liquid flow regimes in bubble column reactors, Chem. Eng. Sci. 52 (21/22) (1997) 3811–3826.
[38] R. Krishna, M.I. Urseanu, J.M. Van Baten, J. Ellenberger, Rise velocity of a swarm of large bubbles in liquids, Chem. Eng. Sci. 54 (1999) 171–183.
[39] R. Collins, The effect of a containing cylindrical boundary on the velocity of a large gas bubble in a liquid, J. Fluid Mech. 28 (1) (1967) 97–112.
[40] R. Krishna, M.I. Urseanu, J.M. Van Baten, J. Ellenberger, Wall effects on the rise of single gas bubbles in liquids, Int. Commun. Heat Mass Transfer 26 (6) (1999) 781–790.
[41] J. Kawasaki, T. Hayakawa, Direct-contact mass and heat transfer between vapour and liquid with change of phase, J. Chem. Eng. Jpn. 5 (2) (1972) 119–124.
[42] A.H. Luedicke Jr., B. Hendrickson, G.M. Pigott, A method for the concentration of proteinaceous solutions by submerged combustion, J. Food Sci. 44 (1979) 469–1473.
[43] J.W. Zhu, S.C. Saxena, Prediction of gas-phase holdup in a bubble column, Chem. Eng. Commun. 161 (1997) 149–161.
[44] I.G. Reilly, D.S. Scott, J.W. De Bruijn, D. Intyre, The role of gas phase momentum in determining gas hold-up and hydrodynamic flow regimes in bubble column operations, Can. J. Chem. Eng. 72 (1994) 3–12.
[45] R. Krishna, J. Ellenberger, C. Maretto, Flow regime transition in bubble columns, Int. Commun. Heat Mass Transfer 26 (4) (1999) 467–475.
[46] F. Kreith, Principles of Heat Transfer, third ed., Intext Educational, New York, 1973, Chapter 7.
[47] Y.T. Shah, B.G. Kelkar, S.P. Godbole, W.-D. Deckwer, Design parameters estimations for bubble column reactors, AIChE J. 28 (3) (1982) 353–379.
[48] S.C. Saxena, N.S. Rao, Heat transfer and gas holdup in a two-phase bubble column: air–water system—review and new data, Exp. Therm. Fluid Sci. 4 (2) (1991) 139–151.

[49] P.L.C. Lage, Multicomponent droplet vaporisation in convective and radiant fields, DSc thesis, PEQ/COPPE/UFRJ, Rio de Janeiro, RJ, 1992 (in Portuguese).
[50] R.C. Reid, J.M. Prausnitz, B.E. Poling, The Properties of Gases and Liquids, fourth ed., McGraw-Hill, New York, 1987, pp. 657, 669.
[51] J.P. Holman, Heat Transfer, fourth ed., McGraw-Hill, New York, 1976, p. 507.
[52] X. Luo, D.J. Lee, R. Lau, G. Yang, L.-S. Fan, Maximum stable bubble size and gas holdup in high-pressure slurry bubble columns, AIChE J. 45 (4) (1999) 665–680.
[53] C.P. Ribeiro Jr., P.L.C. Lage, Experimental study on bubble size distributions in a direct-contact evaporator, Braz. J. Chem. Eng. 21 (1) (2004) 69–81.
[54] B. Bowonder, R. Kumar, Studies in bubble formation—IV: bubble formation at porous discs, Chem. Eng. Sci. 25 (1970) 25–32.
[55] J.L. Sotelo, F.J. Benitez, J. Beltran-Heredia, C. Rodriguez, Gas hold-up and mass transfer coefficients in bubble columns—1. Porous glass-plate diffusers, Int. Chem. Eng. 34 (2) (1994) 82–89.